

Prototyping of microfluidic systems using a commercial thermoplastic elastomer

Emmanuel Roy · Matthias Geissler ·
Jean-Christophe Galas · Teodor Veres

Received: 21 December 2010 / Accepted: 14 March 2011
© Springer-Verlag 2011

Abstract This article describes the fabrication of microfluidic networks (μ FNs) from a commercially available (styrene)–(ethylene/butylene)–(styrene) (SEBS) block copolymer (BCP). The unique combination of hard and elastomeric properties provided by this material promotes high-throughput replication of fluidic structures using thermoforming technologies, while retaining the advantage of quick and easy assembly via conformal contact, as commonly achieved for devices fabricated from poly(dimethylsiloxane) (PDMS). We employ Versaflex CL30, which is optically transparent, available at low cost (e.g., \$2.50/Lbs), and likely to be compatible with a broad range of biological species. We demonstrate excellent fidelity in replication of fluidic structures using hot embossing lithography in conjunction with a photolithographically prepared Si/SU-8 master mold. Moreover, we introduce rapid prototyping of high-quality structures using an approach that we call soft thermoplastic lithography (STPL). Thanks to the rheological characteristics of the SEBS copolymer, STPL enables thermoforming on a heated master at temperatures around 170°C. Using this approach, replication can be completed within a very short period of time (e.g., less than 3 min) without the need of resorting to pressure- or vacuum-assisted instrumentation. Serving as a proof-of-concept, we devise a μ FN that is suitable for the formation of miniaturized arrays comprising fluorescently labeled oligonucleotides and proteins on hard plastic substrates. Resultant spots are characterized by high fluorescent contrast, excellent edge

definition, and uniform distribution of probes within the modified areas.

Keywords Microfabrication · Thermoplastic elastomers · Hot embossing · Microfluidics

1 Introduction

The development of disposable, low-cost microfluidic devices has become central to progress in a number of areas, including proteomic research, environmental screening, and medical diagnostics. Such devices are attractive as they enable multiple operations to be performed on a single chip, while promoting reduced sample consumption and analysis time (Squires and Quake 2009; Whitesides 2006). To this end, lab-on-a-chip (LOC) systems have mostly been shown to function in conceptual ways, yet their commercialization and widespread use have been hindered by a number of challenges, including the availability of suitable materials and low-cost fabrication technologies as primary concerns. In principle, LOC devices can be made from a number of materials, including both soft and rigid ones. Traditionally, microfluidic devices have been fabricated from silicon or glass. These materials offer high mechanical stability, but are relatively expensive and require sophisticated instrumentation for micromachining. Since the advent of soft lithography (Xia and Whitesides 1998), a broad range of microfluidic systems have been produced in PDMS (mostly Sylgard[®] 184 from Dow Corning Corp.), which provides the appealing ability to reversibly conform to other surfaces, resulting in a water-tight seal (McDonald et al. 2000). PDMS-based devices have been shown, for example, to be effective tools for DNA amplification or hybridization reactions (Zhang

E. Roy (✉) · M. Geissler · J.-C. Galas · T. Veres
Industrial Materials Institute, National Research Council
of Canada, 75 de Mortagne Boulevard, Boucherville,
QC J4B 6Y4, Canada
e-mail: Emmanuel.Roy@imi.nrc-nrc.gc.ca

et al. 2006; Benn et al. 2006). However, PDMS is not very well suited for commercial applications given the relatively elevated cost of the prepolymer components, low throughput of production, and limited stability of modified surfaces (Efimenko et al. 2002; Tserapi et al. 2005; Kim et al. 2001; Lee et al. 2003). Several attempts to use alternative materials that could replace PDMS have been undertaken over the last few years. For example, Rolland et al. (2004) have demonstrated the possibility of valving using soft, photocurable perfluoropolyethers. Fiorini et al. (2004) have used a thermoset polyester resin which allows for creating solvent resistant microfluidic devices with a process that involves casting, UV exposure, and thermal curing steps.

The use of thermoplastic (TP) polymers provides an alternative solution to the fabrication of disposable microfluidic devices. Hard TP polymers such as poly(methylmethacrylate) (PMMA), polycyclic olefin (PCO), polycarbonate (PC), and polystyrene (PS) have been used to this end as they are relatively inexpensive, optically transparent, and durable. Moreover, they support replication of micro- and nanoscale features in a rapid, low-cost fashion using nanoimprint lithography (Chou et al. 1995; Cui and Veres 2006), or HEL (Studer et al. 2002; Cameron et al. 2006; Esch et al. 2003). However, the use of hard thermoplastic materials is constrained by the existing mold making technologies and the lack of convenient methods for bonding. For example, thermal bonding can easily lead to deformation of the structures, while processes such as laser welding or solvent bonding do not preserve the integrity of surface treatments (Rossier et al. 1999a, b; Lei et al. 2004; Lin et al. 2007).

Herein, we propose the use of a commercial SEBS thermoplastic elastomer (TPE) as a more tailored, potentially superior material solution for applications in the microfluidic domain. We thereby extend earlier attempts by Sudarsan et al. (2005) who have synthesized a melt processable elastomer gel for rapid fabrication of complex μ FNs. TPE materials are available at relatively low cost, offering transparency, biocompatibility and flexibility comparable to PDMS, while enabling rapid prototyping using established fabrication schemes (e.g., injection molding and HEL). We demonstrate an enhanced thermoforming method that we call *soft thermoplastic lithography* (STPL), which allows for microstructuration without external pressure or vacuum assistance. With STPL, microfluidic devices can be fabricated within 150 s. For the purpose of this study, we selected Versaflex CL30 as a model compound, and demonstrate the fabrication of a TPE-based microfluidic network (μ FN) for DNA and protein micropatterning on PCO (e.g., Zeonor 1060R) surfaces.

2 Materials and methods

Versaflex CL30 was purchased from GLS Corp. (McHenry, IL), and was used in the form of sheets (e.g., 1.0–3.0 mm in thickness, 150 mm in width, and >10 m in length) prepared by extrusion using a Killion KL100 single screw extruder (Killion Laboratories, Inc., Houston, TX). For thermoforming, 4" TPE sheets were cut from the extruded roll and successively rinsed with deionized (DI) water (18.2 M Ω cm), isopropanol (Fisher Scientific, Ottawa, ON) and methanol (Fisher), followed by drying with a stream of nitrogen gas. Optical transmission spectra were collected from polymer sheets (1.0 mm in thickness) using a Beckman DU-640 spectrometer. Mechanical and thermal characterization was carried out with a dynamic mechanical thermal analyzer (DMTA, ARES LS2 rheometer, Rheometric Scientific, Piscataway, NJ). Elastic moduli were determined at 1 Hz with a strain of 0.02% and a heating rate of 2°C min⁻¹.

The master mold was fabricated by standard SU-8 photolithography. SU-8 (e.g., GM1040) resist (Gersteltec, Pully, Switzerland) was spin-coated on a 4" silicon wafer (Silicon Quest International, Inc., Santa Clara, CA) to achieve a layer thickness of 4.2 μ m, followed by pre-bake steps at 65 and 95°C for 5 and 15 min, respectively. The resist layer was exposed to UV light (Hg i-line) through a laser-written high-definition sodalime photomask (HTA Photomask, San José, CA) using an EVG 6200 mask aligner (EV Group, Schärding, Austria). For the post-exposure bake, the same conditions were applied as for the pre-bake. Resist was developed in propylene glycol monomethyl ether acetate (Sigma–Aldrich Corp., St. Louis, MO) and then hard-baked overnight at 160°C. The master was finally treated with trichloro(1*H*,1*H*,2*H*,2*H*-perfluorooctyl)silane (Sigma–Aldrich) to generate an anti-adhesive layer. HEL was carried out using an EVG 520 HE system (EV Group) with a primary vacuum of 0.1 mbar. For STPL, TPE sheets were manually placed onto the SU-8 master and heated to 170°C on a hot plate for 150 s.

Roughness measurements were performed using a multi-mode Nanoscope IV atomic force microscope (AFM, Veeco Metrology Group, Santa Barbara, CA), operated at ambient conditions and in contact mode using silicon nitride cantilevers (NP-S20, Veeco) with a spring constant of 0.58 N m⁻¹. Plasma oxidation (Plasmalab80, Oxford Instruments, Bristol, UK) of TPE was done for 4 min at a gas flow of 20 sccm, a power of 70 W, and a pressure of 50 mTorr. Contact angles were measured with a goniometer from Kerenco Instruments, Inc. (El Paso, TX) using DI water as the probe liquid. Scanning electron microscopy (SEM) images were taken using an S-4800 scanning electron microscope (Hitachi, Mississauga, ON).

Zeonor 1060R was purchased from Zeon Chemicals (Louisville, KY) and has been subjected to thermoforming using an Engel 150T injection molding tool (Engel, Inc., Schwertberg, Austria). Entry ports in array format have been drilled into plastic substrates ($50 \times 75 \text{ mm}^2$ in area) using a Sherline 2000 CNC machine (Sherline, Inc., Vista, CA). Zeonor substrates were exposed to ozone gas for 20 min using an Ozo 2vtt ozone generator (OzoMax, Inc., Shefford, QC), and subsequently incubated with a solution of 8 mg 1-ethyl-3-(3-dimethylaminopropyl)carbodiimide (Sigma–Aldrich) and 2 mg *N*-hydroxysuccinimide (NHS, Sigma–Aldrich) in 100 μl of phosphate buffered saline (PBS, Sigma–Aldrich, pH 7.4) solution for 1 h. Oligonucleotides were purchased from Integrated DNA Technologies, Inc. (Coralville, IA), and were used at a concentration of 32 μM in PBS. Proteins were obtained from Jackson ImmunoResearch Laboratories, Inc. (West Grove, PA), and used at a concentration of 2.0 mg ml^{-1} in PBS. Devices were loaded with $\sim 200 \text{ nl}$ solution using hydrophobic slotted pins (stainless steel, FP3S500H, VP Scientific, Inc., San Diego, CA). Fluorescence imaging of spotted arrays was performed using an Eclipse TE2000-U inverted fluorescence microscope from Nikon (Melville, NY).

3 Results and discussion

3.1 Thermo-mechanical, optical, and adhesion properties of TPE materials

For the most part, TPEs are block copolymers (Holden et al. 1996) comprising different monomer sequences that are distributed randomly, statistically, or in large domains through diblock or triblock architectures (Fig. 1a). Versaflex CL30 is composed of both diblock and triblock copolymer types. For SEBS materials with low PS content (10–12%), thermodynamic incompatibility between blocks induces nanophase separation and self-assembly of PS domains into nanometric clusters (typically 10–30 nm in diameter) which are distributed in a three-dimensional fashion with hexagonal symmetry in the rubber matrix of ethylene-butylene (EB), as illustrated in Fig. 1a. This morphological structure provides the basis of the materials performance: rigid PS domains act as junction points that stabilize the polymer matrix, while the EB dominant phase offers elastomeric properties. Moreover, size and cluster distributions potentially promote the TPE surface to be uniform and homogenous at the microfluidic device level (Roy et al. 2008).

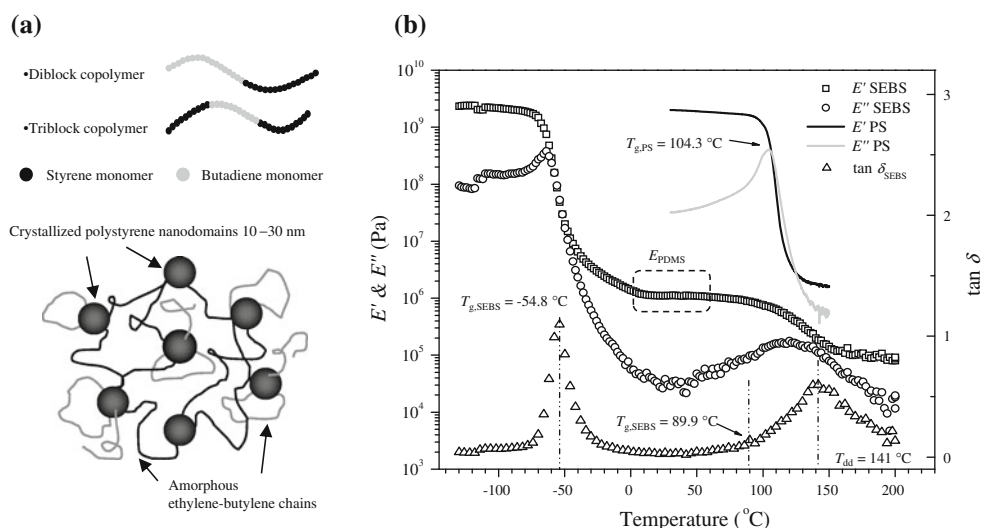
Figure 1b shows the storage (E') and loss (E'') moduli as a function of temperature for SEBS and PS polymers. E' and E'' are a measure of the stored and dissipated energy

related to the elastic and viscous portions, respectively. The ratio of these moduli (E''/E') is the tangent of the phase angle shift (δ) between stress and strain vectors, which characterizes the damping behavior. Following $\tan \delta_{\text{SEBS}}(T)$, the peak at -54.8°C corresponds to the glass transition temperature of the EB soft block ($T_{\text{g,EB}}$), for which ethylene and butylene monomers are distributed in a random fashion. A negative value of $T_{\text{g,EB}}$ is essential for achieving conformal contact and bonding at moderate temperature, as it indicates liquid-like behavior of the material. Above $T_{\text{g,EB}}$, E' reaches a so-called rubber plateau at about 1.16 MPa which extends to 70–80°C. In this regime, E'' is reduced by 2–3 orders of magnitude. The complex Young's modulus which is defined as $E^* = E' + iE''$ is largely comparable to that of standard PDMS (e.g., Sylgard[®] 184), for which the typical range of moduli (e.g., 0.5–2 MPa) is included in Fig. 1b. For neat PS ($\text{MW} = 270 \text{ kg mol}^{-1}$), E' has been measured to be 1.4 GPa at room temperature. In this context, SEBS can be regarded as a hybrid material combining properties of both elastomeric and hard plastic polymers. On one hand, SEBS is almost as soft as PDMS, making it possible to form intimate contact with other surfaces. In fact, contact occurs spontaneously with planar surfaces, and the contact line propagates naturally across the substrates. On the other hand, its block-copolymer structure comprising rigid PS domains provides thermal resistance along with mechanical robustness superior to that of PDMS.

In contrast to thermal bonding of TP materials, which is commonly achieved by a combination of pressure (to maintain surfaces in contact) and thermal activation (to generate inter-diffusion and reorientation of polymer chains), SEBS soft blocks promote effective polymer–polymer interactions at ambient conditions. For this reason, SEBS materials and some of its derivatives are included in many pressure sensitive adhesives, such as the famous Post-it[®] sticker (Trademark of 3M Corp.), which can easily be glued to a broad range of solid supports without mediation by heat, elevated pressure, or solvents. Similar to other adhesives, SEBS materials possess solid and liquid properties alike, which allow for wetting of another surface at the microscopic scale, while maintaining rigidity at the macroscopic level (Creton 2007).

Optical or fluorescence reading on a fluidic chip demands for using materials that provide a high level of transparency, primarily in the UV and visible range. Versaflex CL30 and Zeonor 1060R fulfill this condition (Fig. 2), although at shorter wavelengths both materials are slightly less transparent than PDMS. Defining 50% transmittance as an acceptable limit in transparency, PDMS provides the widest optical window which extends to 280 nm. For Zeonor and Versaflex CL30, 50% transmittance is reached at 340 and 295 nm, respectively. SEBS

Fig. 1 **a** Schematics of styrene/butadiene diblock and triblock polymer chains along with the morphological structure of SEBS block copolymers, in which spherical PS domains are embedded in an amorphous ethylene-butylene matrix with a nearly perfect hexagonal symmetry. **b** Plot of DMTA measurements, indicating E' , E'' and $\tan \delta$ for SEBS and PS. The window illustrates typical values of the Young's modulus for PDMS (e.g., Sylgard® 184) serving as a reference



polymers are clear because PS domains are too small (e.g., 10–30 nm) to scatter light. Another attractive feature of these materials is that they show a relatively low autofluorescence background over a wide spectral range (data not shown).

3.2 Thermoforming of TPE

We fabricated fluidic structures using standard vacuum-assisted HEL and STPL (Fig. 3). For both processes, TPE pieces were cut with scissors from a roll of extruded material (Fig. 3a). Extruded sheets can be stored over long periods of time (e.g., several years) without any notable degradation, making it possible to use the material on demand without any time consuming pre-compounding steps.

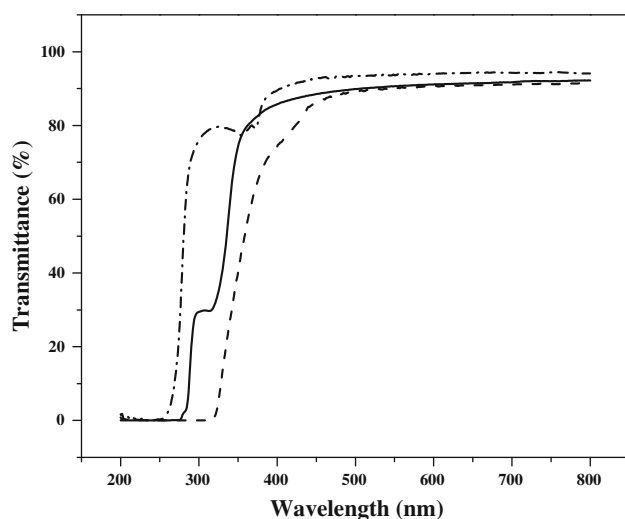


Fig. 2 Optical transmission curves for SEBS (continuous line), PDMS (dashed-dotted line) and Zeonor 1060R (dashed line)

HEL was performed under a primary vacuum of 1 mbar, following the procedure that is outlined in Fig. 3b. In order to select an optimal embossing temperature, the variation in $\tan \delta_{\text{SEBS}}(T)$ offers meaningful insight (Fig. 1b). A barely visible shoulder is observed at 89.9°C and is associated with the glass transition of the PS phase, while the glass transition for neat PS is observed at 104.3°C. The difference in amplitude between the two PS glass transition peaks is related to the ultra-minority fraction of styrene content in SEBS. The difference in temperature of 14.4°C between the two transitions constitutes a “lowering effect” and can be interpreted as a consequence of premature molecular motion in PS domains induced by the poly(ethylene-butylene) segmental mobility (Munteanu and Vasile 2005; Morèse-Séguéla et al. 1980). This observation helps determine embossing parameters and the temperature service for potential applications with the final device.

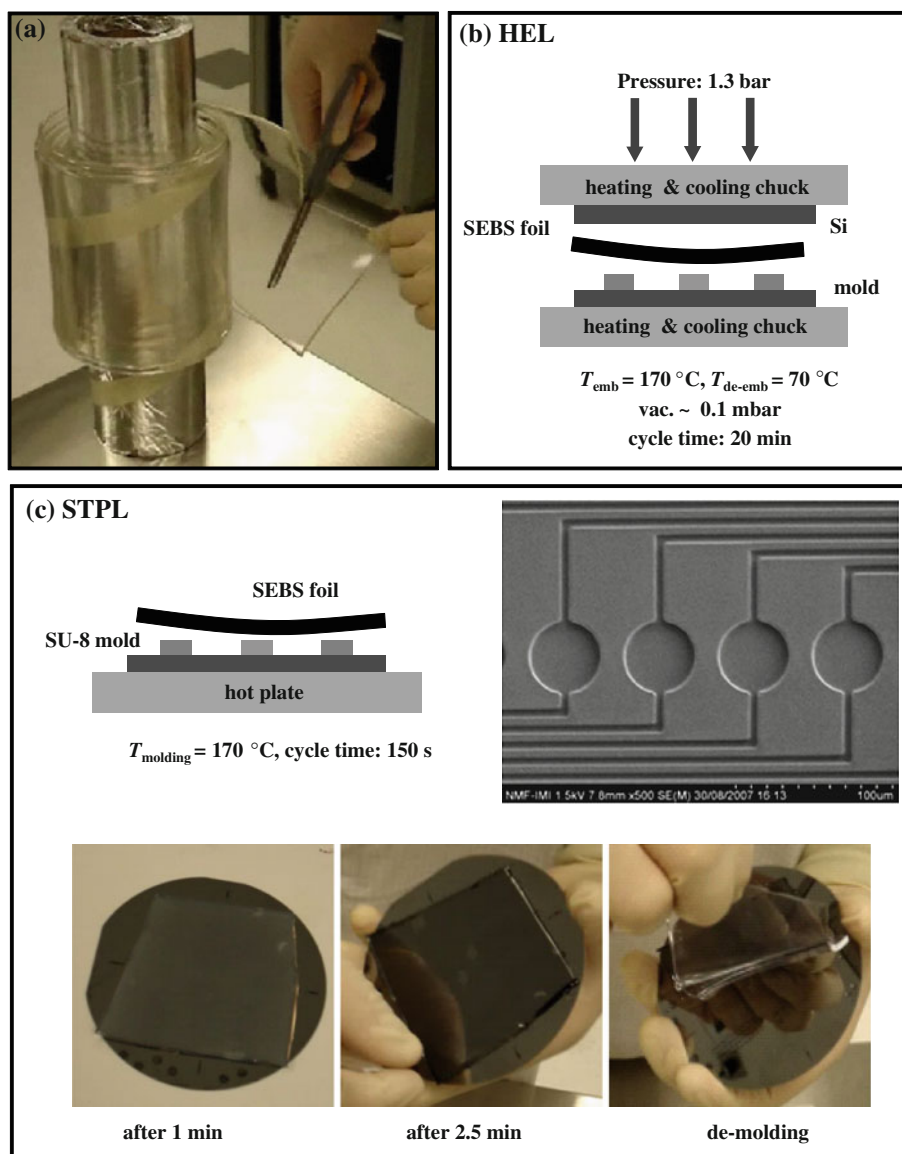
Most work on HEL with hard TP materials (i.e., PMMA, PC, and PS) has been performed at temperatures ranging from 140 to 220°C, following $T_{\text{emb}} = T_g + 40\text{--}90^\circ\text{C}$ as a rule of thumb to obtain a good compromise between temperature and pressure. For styrenic BCPs, determination of optimized T_{emb} diverges from these guidelines. In fact, hard PS nanodomains will not spontaneously dissociate at $T_{g,\text{PS}}$ but gradually deform while keeping their quasi-integrity in the poly(ethylene-butylene) matrix as long as the temperature does not exceed the peak centered at 141°C, which corresponds to the “domain disruption temperature” (T_{dd}) (Wang 2001). Therefore, embossing should be performed at a slightly higher temperature to improve flow behavior and avoid any thermal history effect. Above this transition, E' reaches a plateau region (attained at $\sim 160\text{--}165^\circ\text{C}$) with a stable value of 0.1 MPa, suggesting that an embossing temperature of 170°C should be well suited for high-quality replication. Once top and bottom plates of the embossing machine reach 170°C, a force of 1.0 kN is applied for 2 min.

Fig. 3 a Photograph of an extruded TPE foil on a roll from which pieces can be cut conveniently before use.

b Schematic representation of HEL with a foil of TPE.

c Illustration of STPL.

Photographic insets reveal the changes in transparency for a TPE sheet that undergoes heating and subsequent cooling over a period of 150 s. SEM image of an SEBS μ FN that consists of 5- μ m-wide microchannels connected to 45 μ m circular structures (4.2 μ m in depth) realized at 170°C by STPL



With the force still maintained, the system is cooled to 75°C, followed by release of the pressure. Upon removal of the stack from the instrument, the embossed TPE sheet is peeled off the mold. The shape of the replicated motifs is well-defined, indicating a high level of fidelity that can be achieved with this approach. Moreover, the surface is smooth and free of defects, displaying roughness values of 1.5 and 3.0 nm for areas that were in contact with silicon and SU-8 portions of the mold, respectively. When coated with an anti-sticking layer, we were able to reuse a single mold for many replications (e.g., between 50 and 100 times) without inducing any notable damage to the photoresist features. Similar to PDMS and other elastomers, Versaflex CL30 can be stretched, thus facilitating proper release from the mold.

High-quality replication with PMMA has been realized at 180°C and a pressure of 100 bar (Studer et al. 2002). Cameron et al. (2006) have reported optimized conditions

for PCO materials with an embossing temperature of 40–70°C above T_g and applied forces of 10–20 bar. TPE replication takes advantage of mechanical moduli that are typically 2–3 orders of magnitude lower than those of hard thermoplastics. According to Stefan's equation, the force required for polymer micro-displacement is linearly proportional to the zero shear viscosity parameter (η_0) (Sotomayor Torres 2003). For PMMA, PS, and PC, which come at a molecular weight of several hundred thousand g mol^{-1} and typical low shear rate values of 10^{-4} – 10^{-1} s^{-1} , η_0 ranges from 10^5 to 10^{10} Pa s . Therefore, several tenths of bars need to be applied for inducing polymer displacement rates in the range of $1 \mu\text{m s}^{-1}$ (Yao et al. 2007; Juang et al. 2002). In contrast, soft BCP-TPE materials (with a percentage of hard PS less than 15) show values of η_0 in between 10^2 and 10^4 Pa s (Sebastian et al. 2002a, b). Based on these reports, we can assume that zero shear viscosity

values can be 3–6 orders of magnitude lower for BCP-based TPE than those of hard TP, thus explaining the attractive processing conditions, such as short embossing time and low pressure needed for high-quality replication.

These mechanical and viscoelastic properties pave the way for the development of a simple and low-cost fabrication method accessible to any laboratory that we call soft thermoplastic lithography. As illustrated in Fig. 3c, a TPE sheet is first placed on the Si/SU-8 mold during which an almost perfect contact is achieved. The stack is then heated on a hot plate to 170°C for 150 s (or longer whenever necessary). At this temperature, the TPE material turns opaque due to coalescence of the PS nanodomains, accompanied by a considerable decrease in viscosity. The 3-mm -thick TPE sheet we employed herein generates sufficient pressure (~ 50 Pa) to ensure polymer displacement over micrometer distances. At the same time, we observed that the remaining air bubbles trapped between the mold and the polymer sheet disappeared, which indicates a relatively high gas permeability of the TPE material at elevated temperatures. In crystallized state, PS nanodomains interrupt the gas flow and retard permeation in comparison to the soft and more permeable EB polymer blocks. Although TPE materials are diverse in composition, chemistry, and morphology, the literature suggests that permeability coefficients for nitrogen and oxygen gas at room temperature can be 20–400 times lower than that of PDMS (Odani et al. 1977; Senuma 2000). Upon completion of the thermoforming process, the stack is immersed in water for rapid cooling, and the patterned elastomer sheet is removed from the mold (Fig. 3c). SEM investigation revealed that fluidic structures were replicated with excellent fidelity, showing no difference when compared to replications performed by HEL. As for HEL, we were able to use the same mold for a large number of replication cycles (e.g., >50) while retaining consistent quality of resultant replicas.

3.3 TPE surface treatment and device assembly

Pristine surfaces of Versaflex CL30 are hydrophobic and exhibit advancing (θ_{adv}) and receding (θ_{rec}) contact angles of $106 \pm 2^\circ$ and $84 \pm 3^\circ$, respectively (Fig. 4). This implies that active pumping would be required for fluidic manipulation of aqueous solutions, which might complicate integration, especially when a large number of independent probes were to be used in parallel. Surface hydrophilization provides an alternative as it allows for capillary flow of polar solvents without the need of adding any surfactants. Hence, we investigated treatment of TPE with O_2 plasma and followed the evolution of θ_{adv} and θ_{rec} using DI water (Fig. 4). Initial values of 65° and 27° for θ_{adv} and θ_{rec} are indicative of medium hydrophilicity, resulting from the relatively moderate plasma conditions

employed for treatment. When stored at ambient conditions, the polymer surface undergoes hydrophobic recovery for which three different regimes can be distinguished. The first regime extends over a period of 2–3 days and is characterized by relatively stable contact angles. The second regime continues over another 3 days and involves accelerated loss in hydrophilicity. Finally, values equilibrated at around 79° and 44° over the following 2 weeks.

The contact angle hysteresis shortly after exposure was $\sim 40^\circ$, and therefore $\sim 20^\circ$ higher than that of the pristine surface. For comparison, the contact angle hysteresis for O_2 plasma-treated PDMS is $10\text{--}30^\circ$ (Donzel et al. 2001). We attribute the relatively large contact angle hysteresis to both chemical heterogeneities and nanoscale roughness induced by plasma exposure. AFM measurements indeed confirmed that roughness increased during treatment, resulting in 3.5 and 6.5 nm for surfaces initially in contact with silicon and SU-8 features on the mold. Unlike plasma exposure of PDMS, which results in the formation of a thin, but rather brittle silica layer that tends to generate cracks, plasma treatment of TPE is accompanied by the conversion of hydrocarbon units into hydrophilic groups, such as carboxylic acid. The density of functional groups and hence the wetting properties of resultant surfaces generally depend on the plasma conditions, for which a detailed investigation is yet to be achieved. Overall, plasma hydrophilization proved suitable for autonomous filling of channels up to 10 cm in length ($4\ \mu\text{m}$ in depth), even few days after the plasma treatment.

Plasma treatment did not compromise mechanical and viscoelastic properties of Versaflex CL30, allowing for

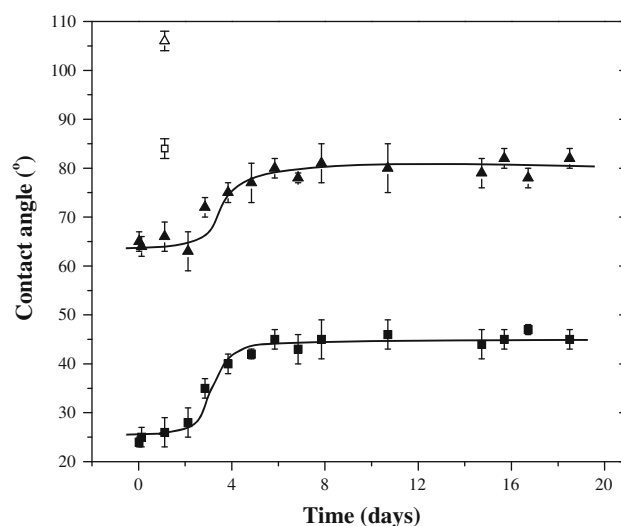


Fig. 4 Evolution of θ_{adv} (filled triangles) and θ_{rec} (filled squares) of DI water for SEBS treated with O_2 plasma for 4 min at a power of 70 W and a gas flow of 20 sccm. Contact angles of non-treated TPE are included as a reference (open triangle and open square symbols is for θ_{adv} and θ_{rec} , respectively). Values are averaged from five measurements; standard deviations are below $\pm 5^\circ$

intimate contact to occur spontaneously across the entire surface when placed on a solid support. However, contact is reversible, and the SEBS layer can be peeled off the substrate at any time. The actual bonding strength between Versaflex CL30 and Zeonor remains variable depending on the temperature and the duration of contact. The example shown in Fig. 5 has been realized without heating or applied pressure, representing a unique and convenient demonstration of a hybrid, all-thermoplastic microfluidic device. The absence of any transition zone between the two materials indicates a high degree of conformity. Moreover, embedded microchannels do not show any signs of deformation. The material therefore seems suitable for assembly and bonding of thermoplastic-based μ FNs without the need for sophisticated equipment or surface treatment processes.

3.4 Spotting and characterization of DNA and protein microarrays

Figure 6 illustrates the spotting approach being investigated in this study. The μ FN (Fig. 6a) supports long-range capillary action (i.e., the autonomous movement of liquid in microchannels) as the sole driving force for fluid manipulation. The design has been adjusted to accommodate transfer of small volumes (e.g., ~ 200 nl) of liquid from a micropin to the inlet structures. In practice, loading is achieved from the backside using a substrate with through-holes, enabling the pin to access the circular, flow-promoting inlet regions of the μ FN. The network of microfluidic channels converges to an array of circular cavities defining the area of the spots to be produced. Each circle is $45 \mu\text{m}$ in diameter and connected to incoming and outgoing channels that are $5 \mu\text{m}$ in width. Circular features are linearly arranged in rows with a periodicity of $60 \mu\text{m}$.

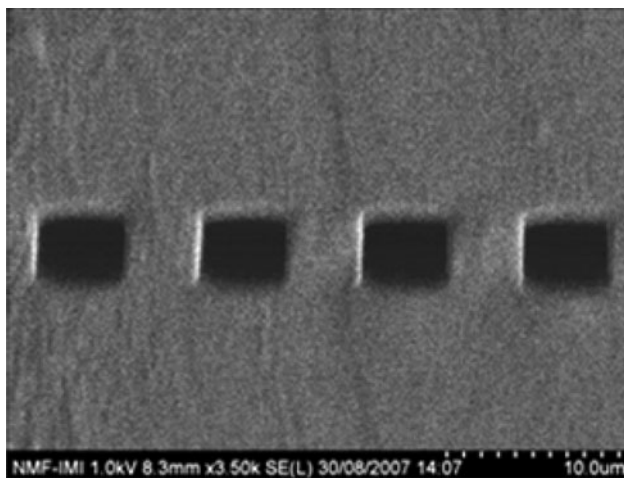


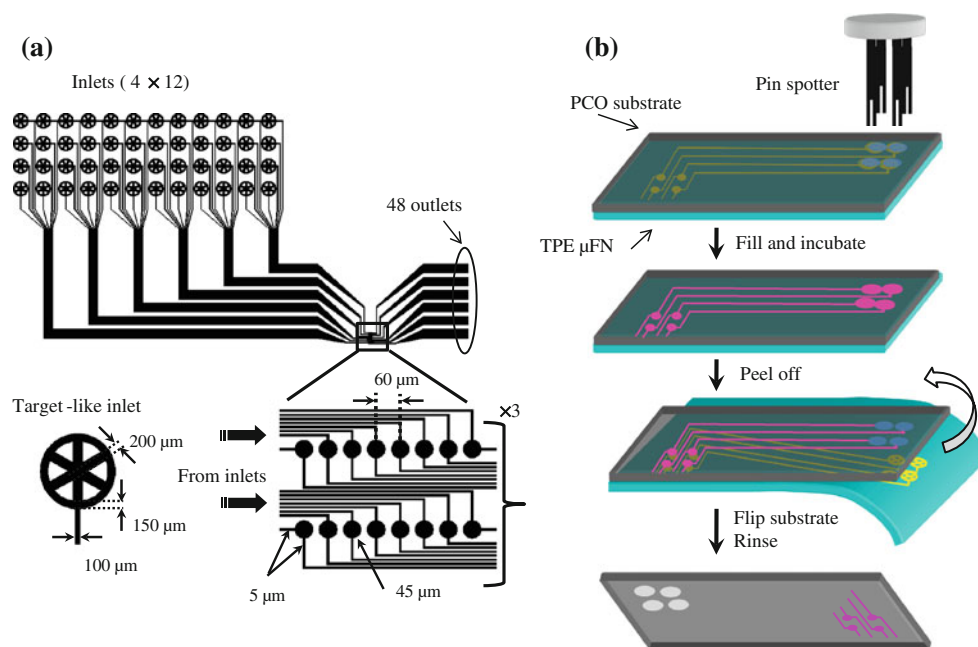
Fig. 5 Cross-sectional view of embedded microchannels (4.2 and $5 \mu\text{m}$ in depth and width, respectively) obtained by bonding of an SEBS μ FN to a Zeonor substrate (previously treated with UV/O_3) at room temperature

The spacing between rows is $200 \mu\text{m}$. PCO substrates have been activated to achieve covalent attachment of amino-modified oligonucleotides and proteins using procedures that were published previously (Diaz-Quijada et al. 2007).

The procedure for patterned, microfluidic immobilization consists of four steps which are illustrated in Fig. 6b. First, the microfluidic TPE layer is placed channel-side down onto the activated substrate which comprises an array of open access holes. The mechanical properties of the TPE promote intimate contact with the substrate, leading to a perfect but non-permanent seal of the two thermoplastic surfaces. An array of hydrophobic pins is used to deliver a solution to the inlet holes. We employed a home-built, computer-assisted x -, y -, z -translation stage which allows for parallel transfer of multiple probes, while promoting accurate positioning of the pins with respect to the microfluidic inlets. The time-dependency of liquid propagation along trajectories ($L(t)$) can broadly be described by Washburn's equation, $L^2 = \gamma Dt/4\eta$, where γ is the surface tension, D is the capillary diameter, and η is the viscosity of the fluid (Washburn 1921). Even though $L(t)$ may encounter limitations for complex and long μ FNs, autonomous filling of microfluidic systems remains convenient even at extended levels of integration (Juncker et al. 2002; Zimmermann et al. 2007). Upon completion of the filling process, the solution is incubated for 16–24 h during which immobilization of DNA or protein takes place through displacement of NHS ester groups and the formation of stable amide bonds (Diaz-Quijada et al. 2007; Johnsson et al. 1991). Finally, the μ FN is removed and un-reacted molecules are washed off the substrate.

Figure 7a shows a 48-spot array composed of two oligonucleotide probes, $5'$ -Cy3-TTT TTT TTT T-(CH_2) $_6$ - NH_2 - $3'$ (P1) and $5'$ -Cy5-TTT TTT TTT TTT TTT-(CH_2) $_6$ - NH_2 - $3'$ (P2), independently immobilized on the surface of Zeonor 1060R. Probes were arranged in a binary fashion, diagonally dividing the array into two different sections. Fluorescence emission was confined to the exposed areas of the surface, which contrasted well with the bare plastic substrate. The transition zone between modified and non-modified regions is relatively short (e.g., $<5 \mu\text{m}$) for the surrounding surface remains efficiently sealed by the elastomer. No defect is apparent in the depicted array. The number of spots showing signs of cross-talk (e.g., Cy3 and Cy5 signals being present in the same area) was below 5%, on average. The image in Fig. 7a further illustrates that fluorescence emission was largely uniform among spots in the array, although fluorescence intensity decreased from left to right (e.g., by $\sim 20\%$ for P1 and $\sim 30\%$ for P2). This finding was systematic for arrays being produced in this way, since the solution partially depletes when moving along the trajectory (Geissler et al. 2009). Figure 7b depicts two randomly selected spots and a plot of their respective intensity

Fig. 6 Spotting with a TPE-based μ FN. **a** Design of the μ FN with detailed views of inlet and immobilization areas. **b** The spotting procedure involves (i) placement of the soft μ FN on an activated Zeonor substrate having access holes, (ii) loading of each channel with 200 nl solution using an array of micropins, (iii) incubation, and (iv) removal of the μ FN, followed by washing non-immobilized molecules off the surface



profiles. Each spot shows a narrow range of signal intensities (e.g., 71 ± 5 and 59 ± 6 units for P1 and P2, respectively), suggesting homogeneous distribution of oligonucleotide probes within the modified regions. Achieving this level of uniformity was promoted in part by the confinement of liquid within the μ FN and the absence of de-wetting and evaporation effects during incubation. In addition to DNA, we probed the patterning of proteins on a plastic support using a similar μ FN. The example shown in Fig. 7c was produced by filling independently 35 pre-selected channels with a solution containing fluorescently labeled immunoglobulin G (IgG) antibodies. The spots that were formed during the exposure faithfully revealed the letters “IMI” in an otherwise dark matrix of unmodified regions. As for oligonucleotides, we were able to achieve homogeneous spots of proteins immobilized on the plastic surface with a high degree of uniformity over the entire array.

4 Conclusion

This article demonstrates that commercial TPE constitutes an appropriate material for fabricating microfluidic devices in a convenient, low-cost fashion. The combination of elastomeric and thermoplastic properties together makes these materials potential substitutes to PDMS or hard TP polymers that are commonly employed to this end. Unlike PDMS, TPE can be used in the form of extruded sheets that provide off-the-shelf availability without the necessity of performing any pre-compounding step. The formation of microstructures in TPE sheets using STPL seems to be an

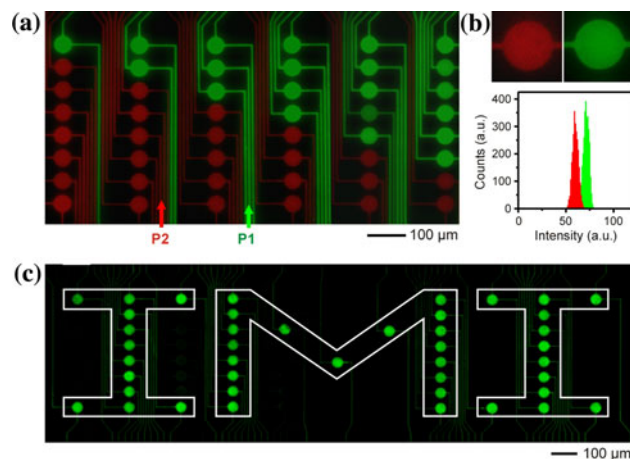


Fig. 7 Fluorescence microscope images of Cy3- and Cy5-labeled oligonucleotides and proteins in array format on NHS-activated Zeonor 1060R substrates. **a** Binary array of 48 spots containing sections of P1 (light grey, above diagonal) and P2 (dark grey, below diagonal), respectively. **b** Close-up views of individual spots along with their corresponding histograms. Fluorescence intensities were adjusted arbitrarily during image acquisition. **c** Array of Cy3-conjugated IgG (sheep anti-mouse) in the form of the letters “IMI”, illustrating the level of control achievable for generating a larger number of spots using this approach

appealing alternative to HEL. With STPL, features can be replicated in less than 3 min over 4" wafer scales without any specialized equipment. Since imprinted SEBS sheets can easily be peeled off the mold, it is possible to use photolithographically prepared Si/SU-8 master molds instead of metallic templates that are traditionally employed for thermoforming of hard TP polymers, adding to the overall cost advantage of the process. We believe that Versaflex CL30 should be suitable for supporting

small-scale features that extend well into the sub-micrometer range, yet the limits in resolution achievable with this material remain to be explored.

Assembly of fluidic devices was done by bonding the TPE sheet onto a PCO substrate, which can be performed at room temperature and without mediation by solvents or external pressure. In fact, the viscoelastic nature of the SEBS material allows for reorganization of chains so that they can adapt to another surface, yielding intimate contact without leakage. While the bonding strength between the two materials allowed for convenient handling, contact was fully reversible at any time, making it possible to correct for misalignment during the assembly process or reuse fluidic devices multiple times. The μ FN developed in the course of this study proved practical to the immobilization of DNA and proteins in array format on a plastic support.

The demonstrations presented in this article suggest that TPE materials open a way for both rapid prototyping and mass production of all-thermoplastic LOC systems. Beyond this economic and rather technological incentive, SEBS materials offer a promising avenue for the fabrication of complex and more sophisticated μ FNs. For example, the possibility of creating multilevel structures for the integration of pneumatically driven valves, pumps, and mixers in a thermoplastic microfluidic device is an interesting option (Roy et al. 2010a). Beyond Versaflex CL30, we have explored other TPE materials for high temperature applications, supporting, for example, polymerase chain reaction-based amplification of DNA (Roy et al. 2010b). It is also clear that for the development of integrated fluidic devices, a number of other material properties need to be considered that were beyond the scope of this study. This includes, for example, permeability or resistance to solvents, diffusion behavior of small molecules, or compatibility with biological processes involving active proteins or live cells. While oxygen plasma proved useful for tailoring wetting properties to some extent, complementary or alternative surface modification schemes may have to be developed to promote a widespread acceptance of SEBS materials for soft microfabrication.

Acknowledgments We thank our colleagues H el ene Roberge, Fran ois Normandin, Kien Mun Lau, Yves Simard, and Pierre Sammut for technical assistance as well as R egis Peytavi, Gerardo A. Diaz-Quijada and Daniel C. Tessier for useful discussion. This work was supported in part by the National Research Council of Canada, G enome Qu ebec and Genome Canada.

References

- Benn JA, Hu J, Hogan BJ, Fry RC, Samson LD, Thorsen T (2006) Comparative modeling and analysis of microfluidic and conventional DNA microarrays. *Anal Biochem* 348:284–293
- Cameron NS, Roberge H, Veres T, Jakeway SC, Crabtree HJ (2006) High fidelity, high yield production of microfluidic devices by hot embossing lithography: rheology and stiction. *Lab Chip* 6:936–941
- Chou SY, Krauss PR, Renstrom PJ (1995) Imprint of sub-25 nm vias and trenches in polymers. *Appl Phys Lett* 67:3114–3116
- Creton C (2007) Block copolymers for adhesive applications. In: Matyjaszewski K, Gnanou Y, Leibler L (eds) *Macromolecular engineering: precise synthesis, materials properties and applications*. Wiley-VCH, Weinheim, pp 1731–1752
- Cui B, Veres T (2006) Pattern replication of 100 nm to millimeter-scale features by thermal nanoimprint lithography. *Microelectr Eng* 83:1299–1305
- Diaz-Quijada GA, Peytavi R, Nantel A, Roy E, Bergeron MG, Dumoulin MM, Veres T (2007) Surface modification of thermoplastics—towards the plastic biochip for high throughput screening devices. *Lab Chip* 7:856–862
- Donzel C, Geissler M, Bernard A, Wolf H, Michel B, Hilborn J, Delamarche E (2001) Hydrophilic poly(dimethylsiloxane) stamps for microcontact printing. *Adv Mater* 13:1164–1167
- Efimenko K, Wallace WE, Genzer J (2002) Surface modification of Sylgard-184 poly(dimethyl siloxane) networks by ultraviolet and ultraviolet/ozone treatment. *J Colloid Interface Sci* 254:306–315
- Esch M, Kapur S, Irizarry G, Genova V (2003) Influence of master fabrication techniques on the characteristics of embossed microfluidic channels. *Lab Chip* 3:121–127
- Fiorini GS, Lorenz RM, Kuo JS, Chiu DT (2004) Rapid prototyping of thermoset polyester microfluidic devices. *Anal Chem* 76:4697–4704
- Geissler M, Roy E, Diaz-Quijada GA, Galas J-C, Veres T (2009) Microfluidic patterning of miniaturized DNA arrays on plastic substrates. *ACS Appl Mater Interfaces* 1:1387–1395
- Holden G, Legge NR, Quirk R, Schroeder HE (1996) *Thermoplastic elastomers*, 2nd edn. Hanser/Gardner, Cincinnati
- Johnsson B, L of as S, Lindquist G (1991) Immobilization of proteins to a carboxymethyl-dextran-modified gold surface for biospecific interaction analysis in surface plasmon resonance sensors. *Anal Biochem* 198:268–277
- Juang YJ, Lee LJ, Koelling KW (2002) Hot embossing in microfabrication. Part I: experimental. *Polym Eng Sci* 42:539–550
- Juncker D, Schmid H, Drechsler U, Wolf H, Wolf M, Michel B, de Rooij N, Delamarche E (2002) Autonomous microfluidic capillary system. *Anal Chem* 74:6139–6144
- Kim J, Chaudhury MK, Owen MJ, Orbeck T (2001) The mechanisms of hydrophobic recovery of polydimethylsiloxane elastomers exposed to partial electrical discharges. *J Colloid Interface Sci* 244:200–207
- Lee JN, Park C, Whitesides GM (2003) Solvent compatibility of poly(dimethylsiloxane)-based microfluidic devices. *Anal Chem* 75:6544–6554
- Lei KF, Ahsan S, Budraa N, Li JW, Mai JD (2004) Microwave bonding of polymer-based substrates for potential encapsulated micro/nanofluidic device fabrication. *Sens Actuators A* 114:340–346
- Lin CH, Chao CH, Lan CW (2007) Low azeotropic solvent for bonding of PMMA microfluidic devices. *Sens Actuators B* 121:698–705
- McDonald JC, Duffy DC, Anderson JR, Chiu DT, Wu H, Schueller OJA, Whitesides GM (2000) Fabrication of microfluidic systems in poly(dimethylsiloxane). *Electrophoresis* 21:27–40
- Mor ese-S egu ela B, St-Jacques M, Renaud JM, Prud'homme J (1980) Microphase separation in low molecular weight styrene–isoprene diblock copolymers studied by DSC and ¹³C NMR. *Macromolecules* 13:100–107

- Munteanu SB, Vasile C (2005) Spectral and thermal characterization of styrene-butadiene copolymers with different architectures. *J Optoelectron Adv Mater* 7:3135–3148
- Odani H, Taira K, Nemoto N, Kurata M (1977) Diffusion and solution of gases and vapors in styrene-butadiene block copolymers. *Polym Eng Sci* 17:527–534
- Rolland JP, Van Dam RM, Schorzman DA, Quake SR, DeSimone JM (2004) Solvent-resistant photocurable “liquid teflon” for microfluidic device fabrication. *J Am Chem Soc* 126:2322–2323
- Rossier JS, Bercier P, Schwarz A, Loridant S (1999a) Topography, crystallinity and wettability of photoablated PET surfaces. *Langmuir* 15:5173–5178
- Rossier JS, Roberts MA, Ferrigno R, Girault HH (1999b) Electrochemical detection in polymer microchannels. *Anal Chem* 71:4294–4299
- Roy E, Siegrist J, Peytavi R, Diaz-Quijada GA, Roberge H, Normandin F, Jia G, Zoval J, Madou M, Bergeron MG, Dumoulin MM, Veres T (2008) Thermoplastic elastomers (TPE) block copolymers, a new material platform for microfluidics: proof-of-concept for complex siphon valving on CD. In: Proceedings of the 12th international conference on miniaturized systems for chemistry and life sciences, San Diego, pp 1576–1578
- Roy E, Galas J-C, Veres T (2010a) Thermoplastics elastomers for microfluidics valving and mixing, toward highthroughput fabrication of multilayers devices. In: Proceedings of the 14th international conference on miniaturized systems for chemistry and life sciences, Groningen, pp 1235–1237
- Roy E, Mounier M, Peytavi R, Siegrist J, Gorkin R, Madou M, Bergeron MG, Veres T (2010b) Enhanced microfabrication capabilities of thermoplastics elastomers for CD lab system including: lysing, PCR and hybridization microfluidic functions. In: Proceedings of the 14th international conference on miniaturized systems for chemistry and life sciences, Groningen, pp 1898–1901
- Sebastian JM, Lai C, Graessley WW, Register RA (2002a) Steady-shear rheology of block copolymer melts: zero-shear viscosity and shear disordering in body-centered-cubic systems. *Macromol* 35:2700–2706
- Sebastian JM, Lai C, Graessley WW, Register RA (2002b) Steady-shear rheology of block copolymer melts: zero-shear viscosity and shear disordering in body-centered-cubic systems. *Macromol* 35:2707–2713
- Senuma A (2000) Gas permeability coefficients of ethylene-vinyl acetate copolymer-modified poly(dimethylsiloxane) membranes. Double-column approach for two-phase materials. *Macromol Chem Phys* 201:568–576
- Sotomayor Torres CM (2003) Alternative lithography: unleashing the potentials of nanotechnology. Kluwer, New York
- Squires TM, Quake SR (2009) Microfluidics: fluid physics at the nanoliter scale. *Rev Mod Phys* 77:977–1026
- Studer V, Pépin A, Chen Y (2002) Nanoembossing of thermoplastic polymers for microfluidic applications. *Appl Phys Lett* 80:3614–3616
- Sudarsan AP, Wang J, Ugaz VM (2005) Thermoplastic elastomer gels: an advanced substrate for microfluidic chemical analysis systems. *Anal Chem* 77:5167–5173
- Tseripi A, Gogolides E, Tsougeni K, Constantoudis V (2005) Tailoring the surface topography and wetting properties of oxygen-plasma treated polydimethylsiloxane. *J Appl Phys* 98:113502.1–113502.6
- Wang C (2001) Tear strength of styrene-butadiene-styrene block copolymers. *Macromol* 34:9006–9014
- Washburn EW (1921) The dynamics of capillary flow. *Phys Rev* 17:273–283
- Whitesides GM (2006) The origins and the future of microfluidics. *Nature* 442:368–373
- Xia Y, Whitesides GM (1998) Soft lithography. *Angew Chem Int Ed* 37:551–575
- Yao D, Nagarajan P, Li L, Yi AP (2007) A two-station embossing process for rapid fabrication of surface microstructures on thermoplastic polymers. *Polym Eng Sci* 47:530–539
- Zhang C, Xu J, Ma W, Zheng W (2006) PCR microfluidic devices for DNA amplification. *Biotechnol Adv* 24:243–284
- Zimmermann M, Schmid H, Hunziker P, Delamarche E (2007) Capillary pumps for autonomous capillary systems. *Lab Chip* 7:119–125